ACS SENSORS

pubs.acs.org/acssensors

Article

HologLev: A Hybrid Magnetic Levitation Platform Integrated with Lensless Holographic Microscopy for Density-Based Cell Analysis

Kerem Delikoyun,[‖] Sena Yaman,[‖] Esra Yilmaz, Oyku Sarigil, Muge Anil-Inevi, Kubra Telli, Ozden Yalcin-Ozuysal, Engin Ozcivici, and H. Cumhur Tekin*

Cite This: *ACS Sens.* 2021, 6, 2191−2201

Read Online

ACCESS | Metrics & More | Article Recommendations | Supporting Information

ABSTRACT: In clinical practice, a variety of diagnostic applications require the identification of target cells. Density has been used as a physical marker to distinguish cell populations since metabolic activities could alter the cell densities. Magnetic levitation offers great promise for separating cells at the single cell level within heterogeneous populations with respect to cell densities. Traditional magnetic levitation platforms need bulky and precise optical microscopes to visualize levitated cells. Moreover, the evaluation process of cell densities is cumbersome, which also requires trained personnel for operation. In this work, we introduce a device (HologLev) as a fusion of the magnetic levitation principle and lensless digital inline holographic microscopy (LDIHM). LDIHM provides ease of use by getting rid of bulky and expensive optics. By placing an imaging sensor just beneath the microcapillary channel without any lenses, recorded holograms are processed for determining cell densities through a fully automated digital image processing scheme. The device costs less than $100 and has a compact design that can fit into a pocket. We perform viability tests on the device by levitating three different cell lines (MDA-MB-231, U937, D1 ORL UVA) and comparing them against their dead correspondents. We also tested the differentiation of mouse osteoblastic (7F2) cells by monitoring characteristic variations in their density. Last, the response of MDA-MB-231 cancer cells to a chemotherapy drug was demonstrated in our platform. HologLev provides cost-effective, label-free, fully automated cell analysis in a compact design that could be highly desirable for laboratory and point-of-care testing applications.

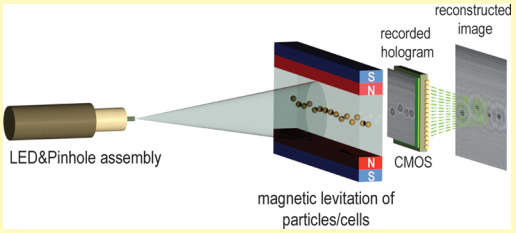

KEYWORDS: *magnetic levitation, holographic microscopy, density-based separation, cell analysis, drug testing, single-cell monitoring, label-free analysis*

Global healthcare becomes more decentralized each year owing to the cost of delivering effective diagnostics and therapeutic services at central medical institutions, which gradually lead to adapting some of the most crucial diagnostic tests into portable, rapid, and economically desirable devices.[1] However, the identification of target cells within heterogeneous cell populations or bodily fluids (e.g., blood) remains as an important goal for a variety of clinical testing. Gold standard techniques for cell separations heavily rely on some well-known biophysical or biochemical aspects of cells, such as size, density, or surface receptor markers of cells.[2] Biochemical or immunoassays require high-cost reagents, bulky and precise instrumentation, and trained personnel, conditions which can be supported at the institutional level. Furthermore, cell labeling protocols are labor-intensive and expensive procedures.[3] On the other hand, separating target cells using biophysical properties is a low-cost, rapid, and simple method to be deployed in a wide range of facilities. However, some of the biophysical properties such as size difference may not be suitable for purifying target cells.[4] One of the most widely used techniques for cell separation is the differences in the density.[5] Density differences within cell populations may occur based on biochemical and genetic factors, such as differential gene expression and energy consumption.[6,7] Although such differences in density among cell populations are quite low, they can be utilized for separation at the single cell level.[8] Most widely used methods for determining the density of cell populations are Ficoll gradient centrifugation[9] and dielectrophoretic field-flow fractionation,[10] none of which allow measurement of cell density at the single cell level, and thus, it is unlikely to separate the target organism at the single cell level by using these techniques. Recently, magnetic levitation has shown superior performances to traditional density-based separation techniques that it enables measurement of cell density at the single cell level by precisely balancing forces acting on each cell at the microscale.[8] Each cell is levitated to suspend at a unique height directly related with the density. Thus, magnetic levitation offers whole new possibilities for separation of rare cells, which has clinically relevant prognostic value for personalized medicine.

Received: December 10, 2020
Accepted: June 2, 2021
Published: June 14, 2021

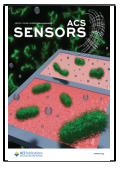

https://doi.org/10.1021/acssensors.0c02587
ACS Sens. 2021, 6, 2191−2201

Magnetic levitation has been an attractive tool for researchers from a variety of disciplines in life sciences[11] due to its simplicity, cost-effectiveness, and minimal effort for processing of the sample, but above all, the major advantage is to provide label-free separation of target cells in a heterogeneous solution. So far, a wide range of applications including label-free separation of malaria-infected red blood cells, sickle cells,[12] blood,[12,13] tumor cells,[8,13] adipocytes,[14] and cardiomyocytes,[15] realization of microparticle-based immunoassays,[16,17] and biofabrication of cells[18−20] has been achieved by applying magnetic levitation technology.

Traditionally, magnetic levitation platforms rely on bulky and costly microscope instruments in order to visualize the sampling chamber for evaluating the positions of cells.[8] Therefore, a microcapillary glass channel containing heterogeneous cell solution is placed between two magnets with the same poles facing each other in a vertical orientation, and two 45° angle tilted mirrors are used on the sides of the microcapillary channel to observe the cells under a microscope. Hence, benchtop and high-cost optical microscopes are required to be operated by trained personnel in a traditional magnetic levitation configuration, which can limit its usage as a standalone device. Since tilted mirrors are used to visualize the capillary channel, the effective working distance of the objectives as well as the distance from the microscope stand to the objective may greatly vary. Hence, the magnetic levitation platform may not be easily compatible with various brands and models of benchtop microscopes and may require additional modifications to utilize for imaging. Several studies aim to deliver portable and low-cost magnetic levitation configurations that can be adapted to a mobile phone camera for visualization. However, these studies can barely resolve features with a size of roughly a white blood cell (∼20 μm) without proper illumination and additional optical configuration providing an effective magnification scheme.[21,22] Thus, smartphone cameras alone may not be a fully end-to-end solution for magnetic levitation in the cellular imaging or biomolecule detection fields. Alternatively, a handheld magnetic levitation platform for point-of-care testing has been shown to provide a low-cost and compact design solution that has the capability to deliver rapid analysis and ease of use; however, this design required manual focusing on microparticles that is incompatible with automated processing.[23] As lensless digital inline holographic microscopy (LDIHM) does not utilize any optics such as lens or mirrors, LDIHM is an attractive image modality for cellular imaging and diagnostic applications, and thus, the increasing number of applications has been demonstrated that LDIHM is a highly suitable choice as a low-cost and handheld cell monitoring device.[24] The light coming from a low-cost, incoherent light source (e.g., light-emitting diode - LED) is spatially filtered by using a relatively large pinhole (∼100 μm in diameter) to illuminate the sample that is directly placed on top of the imaging sensor in close proximity for recording the superimposed wavefront composed of the reference wave, which is undistorted illumination light, and an object wave, which diffracts from the sample.[24] Those two waves sum up at the sensor plane to form the interference pattern also known as a hologram. The recorded hologram is required to be reconstructed to obtain the real image of the sample.[24] Therefore, all these processes are fully digital and automated to eliminate human error and intervention for repeatable and precise measurements.

In this manuscript, we demonstrate the first use of the hybrid cell analysis platform (HologLev) composed from magnetic levitation and lensless digital inline holographic microscope. Cell densities are automatically calculated on the platform from acquired holograms of levitated cells. Holograms are processed by using the Angular Spectrum Method for reconstruction and auto-focusing algorithm, rotation, digital enhancement (e.g., adjusting brightness/contrast and binarization for mask creation), and eventually measurement of levitation heights of cells to calculate density individually automatically in a sequential order. Using HologLev, we tested the viabilities of three different cell lines (i.e., D1 bone marrow stem cells, MDA-MB-231 breast cancer cells, and U937 monocytes), differentiation of a multipotent cell line (i.e., 7F2, mouse osteoblasts), and drug response of MDA-MB-231 cells to a commonly used chemotherapy drug, Docetaxel, by monitoring cell densities. This low-cost standalone platform requires minimal cell preparation protocols and technical expertise that would help to increase dissemination and utilization of magnetic levitation on various cell analysis scenarios. Here, we exploited the synergistic usage of both magnetic levitation technology and lensless holographic microscopy imaging system to obtain a low-cost, portable, and handheld cell, and particle analysis device. We tested the performance of our platform for readily performed assays in magnetic levitation, and we believe that this device could be easily adopted for any magnetic levitation-based cell or particle applications in the future.

MATERIALS AND METHODS

Experimental Setup. The hybrid platform was designed using computer-aided design software, and the main framework of the platform was manufactured by a stereolithography-based 3D printer (Formlabs Form 2), which allows precise manufacturing.[25] After assembling 3D printed parts together, the factory built-in lens of the complementary metal oxide semiconductor (CMOS) imaging sensor (Sony IMX219 - Raspberry Pi camera v2) was detached and the sensor was placed beneath two opposing magnets (N52 grade neodymium magnets, 50 mm length × 2 mm width × 5 mm width, Supermagnete) with a separation gap less than 1 mm. The illumination and recording schemes were designed and built as a connected one piece so that the part can be slidable along the microcapillary channel for visualization of different portions of the channel. The incoming light from a light-emitting diode (LED528EHP, Thor Labs, Newton, NJ) with a central wavelength of 525 nm is spatially filtered by a pinhole with a diameter of 100 μm, which was manufactured by laser cutting machinery to drill the pinhole on a thin slice of aluminum sheet. Then, the light leaves the pinhole and reaches the microcapillary at a distance of about 5 cm so that plane wave approximation was ensured for further imaging processing steps.[26]

Magnetic Levitation Principle. Nonionic paramagnetic solution (Gadavist, Bayer) was utilized to levitate cell samples in the microcapillary placed between two opposing magnets in the magnetic levitation platform that eliminates the need for the use of an external labeling process that provide label-free separation of cells with respect to their densities. This paramagnetic solution has been shown that cell viability and physiology are not adversely affected in elevated concentrations (>100 mM).[18]

In the magnetic levitation platform, cells tend to move to the middle point of the two magnets, where the magnetic field becomes minimum. Then, the cells become stationary when magnetic and buoyancy forces balance each other as in the following equation[8]

$$\frac{V(\chi_c - \chi_m)}{\mu_0}(\vec{B}\cdot\nabla)\vec{B} + V(\rho_c - \rho_m)g = 0 \quad (1)$$

where χ_c and χ_m are the magnetic susceptibilities of cells and paramagnetic medium, μ_0 is the permeability of free space (vacuum)

https://doi.org/10.1021/acssensors.0c02587
ACS Sens. 2021, 6, 2191−2201

(1.2566×10^{-6} kg·m·A^{-2}·s^{-2}), $\vec{B}$ indicates the magnetic induction (T), ρ_c, ρ_m are the densities of cells and medium, g is the gravitational acceleration (9.8 m·s^{-2}), and V is the volume of the cell. As seen in the equation, the V term is cancelled out so that the levitation height profile does not depend on the cell volume. However, cells with bigger diameters come to the equilibrium levitation positions much faster. Moreover, cells have negligible magnetic susceptibility (χ_c) compared to the paramagnetic solution. As a result, if we levitate the cells in the same environment, the main factor that results in unique levitation height profiles is the density of cells. In the platform, denser cells levitate closer to the bottom magnet. Hence, the cell density can be identified by measuring the levitation height (i.e., the distance to the bottom magnet) of the cell.

Image Acquisition. The entire acquisition process was performed with a Raspberry Pi 3 Model B+ by using a fully automated custom-built Python script where the acquisition time and imaging parameters can be adjusted for remote and prescheduled screening and recording schemes. Once the interference pattern between the light diffracted from cells within the microcapillary channel and the undistorted background illumination was acquired, the resultant hologram was reconstructed to obtain real cell images. Thus, the recorded hologram ($\Psi_{Po}(x, y)$) on the sensor plane was back-propagated to the object plane along the z-axis by using a spatial transfer function ($H(k_x, k_y; z)$) with incremental steps (z) to find the focused and high contrast object images by applying an embedded autofocus algorithm.[27] Therefore, the Angular Spectrum Method was used as the back-propagation algorithm, and at each step of z, Fourier transformation of the hologram was performed, and the resultant image was multiplied with transfer function.[24] After applying inverse operation for Fourier transform, the complex-valued image was converted into amplitude and phase images ($\Psi_P(x, y; z)$) by taking the absolute and the argument of the complex-valued image, respectively[24]

$$\Psi_P(x, y; z) = \mathcal{F}^{-1}\{\mathcal{F}\{\Psi_{Po}(x, y)\}H(k_x, k_y; z)\} \tag{2}$$

$$H(k_x, k_y; z) = \left[-jk_o z\sqrt{1 - \frac{(p\Delta_{kx})^2}{k_o^2} - \frac{(q\Delta_{ky})^2}{k_o^2}}\right] \tag{3}$$

$k_o = w_o/v$ is the wavenumber, where w_o is angular frequency (rad/s) and v is the speed of the wavefront. (x, y) and (p, q) are indices for the spatial and Fourier domains of the sample, respectively. $\Delta_{kx} = 2\pi/M\Delta_x$ and $\Delta_{ky} = 2\pi/N\Delta_y$ are the frequency resolutions in the x and y directions (radian per unit of length), where Δ_x and Δ_y are the sampling periods and M, N are the numbers of samples (i.e., pixel counts), respectively.

The amplitude image was used to evaluate if the in-focus image was obtained. The sharpness value of the recent amplitude image was calculated and compared against the previous image. If the value decreased, the recent image should be more in-focus than the previous one, and thus, the value and the image were updated. This process was performed within a certain interval in the z direction to find the optimal distance that matches with the actual object plane for more in focus and sharp reconstructed images.

Automated Analysis of Cell Densities from Images. Once the in-focus amplitude image was obtained, Hough transformation[28] was applied to the image to align the bottom magnet horizontally for further density calculations in latter steps. As reconstructed holographic (i.e., amplitude) images suffer from an optical artifact presented in LDIHM accompanied with a severe irregular background noise, thresholding may become a very challenging task. Thus, a series of morphological operations were performed prior to determining the spatial coordinates of each microparticle. First, the contrast of the image was enhanced in order to relieve the edges, which were suppressed by the noise coming from the overlapped twin image. After creation of a binary mask that indicates the positions of each cell, the center of gravity of each blob (i.e., cell mask) was detected. Accordingly, the vertical distances between calculated coordinates of each blob and the horizontal plane indicating the upper edge of the bottom magnet whose height was automatically determined after Hough transformation.[29] Note that calculated horizontal lines using Hough transform were also used to determine the microcapillary channels' top and bottom contours. Hence, any particle found higher or lower than this region was excluded before density calculations. Therefore, levitation heights of cells were converted into density values by using the calibration curve of polystyrene microspheres with known densities. All computational processes were performed by a custom built script using MATLAB 2018a.

Levitation of Polyethylene Microspheres. Polyethylene microspheres with different densities, 1.00 g mL^{-1} (with size of 10−20 μm), 1.02 g mL^{-1} (with size of 10−20 μm), 1.05 g mL^{-1} (with size of 45−53 μm), and 1.09 g mL^{-1} (with size of 20−27 μm) (Cospheric LLC, ABD), were levitated in phosphate buffered saline (PBS, Gibco) with 1% (w/v) Pluronic F-127 (Sigma Aldrich, Germany) containing 25, 50, 75, and 100 mM gadolinium (Gd^{3+}) (Gadavist, Bayer). Levitation heights of microspheres were measured in the platform after they reached the stationary position in 10 min.

Cell Culture. D1 ORL UVA (mouse bone marrow stem cells) and MDA-MB-231 (breast cancer cells) were cultured in Dulbecco's modified Eagle's high glucose medium (DMEM, Gibco) supplemented with 10% fetal bovine serum (ECS0180, Euroclone) and 1% penicillin/streptomycin (Penicillin/Streptomycin 100×, Euroclone). U-937 human monocyte cells were cultured in a Roswell Park Memorial Institute medium (RPMI-1640, ECM0495L, Euroclone) containing 10% FBS and 1% penicillin/streptomycin. The cells were grown in a humidified 37 °C incubator with 5% CO_2. The growth medium was changed every other day, and the cells were passaged every 4 to 6 days.

7F2 (mouse osteoblasts) cells were grown in a growth medium supplemented with 10% FBS and 1% penicillin/streptomycin at a 5% CO_2 humidified atmosphere at 37 °C. 7F2 cells were cultured in an alpha modified essential medium (αMEM, Sigma Aldrich). The growth medium was refreshed every 2−3 days, and the cells were passaged every 4−6 days. For differentiation of the 7F2 cells into adipocytes, the cells were induced in αMEM with induction agents for 10 days.[14] The adipogenic induction medium was refreshed every 2−3 days. Differentiation of 7F2 cells into adipocytes was determined by a Red oil O stain (Amresco, Solon, OH, USA).

Cell Preparation for Density Analysis in HologLev. Live D1 ORL UVA and MDA-MB-231 cells were trypsinized and spun down at 125g for 5 min, and the supernatant was discarded. U-937 cells were prepared by using the same protocol without trypsinization. The cells were resuspended to 10^5 cells per mL in the culture medium with 25 or 100 mM Gd^{3+}, and then 40 μL of cell solution was loaded into the capillary channel. After 10 min of levitation in HologLev, they were imaged with the integrated LDIHM system.

The levitation profiles of dead D1 ORL UVA, MDA-MB-231, and U-937 were also investigated with 25 and 100 mM Gd^{3+}. To this end, dead cells were obtained by introducing 1:1 (v/v) dimethyl sulfoxide (DMSO, Sigma Aldrich) to cell media. Then, cells were resuspended to 10^5 cells/mL concentration in PBS containing (w/v) 1% Pluronic F-127 with 25 or 100 mM Gd^{3+}. Then, 40 μL of cell sample was loaded into the capillary in the platform and inspected after 10 min of levitation.

Mouse bone marrow osteoblast 7F2 cells that were cultured in the growth and adipogenic induction media were trypsinized on the 15th day and were centrifuged at 125g for 5 min. Then, the culture medium was removed, and the pellet was resuspended to 10^5 cells per mL in the culture medium containing 25 mM Gd^{3+}. 40 μL of sample was loaded into the microcapillary channel for inspection after 10 min of levitation.

Cell Viability Assessment. The cells were stained with Calcein AM/PI solution for 15 min and visualized under a fluorescence microscope. Viability of the cells was analyzed by manually counting live and dead cells.

Calculation of IC_{50} and MTT Assay. MDA-MB-231 cells were seeded at a concentration of 15,000 cells/well into 48-well plates. After 24 h of culture, cells were treated with Docetaxel (ADOOQ) (5−10,000 nM) for 48 h based on the drug half-life. Cell viability was measured with the thiazolyl blue tetrazolium bromide (MTT) assay. 0.5 mg/mL of MTT reagent (Amresco) was added to each well, and the cells were incubated at 37 °C for 4 h in the dark. After the medium was removed, DMSO was added to each well and the absorbance was

https://doi.org/10.1021/acssensors.0c02587
ACS Sens. 2021, 6, 2191−2201

measured at 570 nm with a reference wavelength of 690 nm (Thermo Scientific Multiskan Go). The IC_{50} (the concentration required for 50% inhibition of cell viability) was calculated using the GraphPad Prism 8 software.

2D and 3D Drug Response Experiments. Docetaxel (chemotherapy drug) stock solution was prepared as 10 mM by dissolving in DMSO for drug treatment assays. For 2D treatment, MDA-MB-231 cells were seeded into 6-well plates with a concentration of 10^5 cells/well and cultured for 24 h. Then, the cells were exposed to their IC_{50} Docetaxel dose (63 nM) for 48 h. The cells were trypsinized and collected for analysis in the magnetic levitation platform with 100 mM Gd^{3+}.

For 3D drug treatment, MDA-MB-231 cells prepared as 10^4 cells/mL in the culture medium. Afterward, Docetaxel was directly added to the growth medium at the IC_{50} dose (63 nM), and 40 μL of cell solution with 100 mM Gd^{3+} was loaded into the capillary channel. The cells were levitated in HologLev, which was placed within a cell incubator whose temperature was set to 37 °C. Cells were monitored in the platform to assess the effect of drug treatment for 72 h.

Statistical Analysis. Live and dead cells of D1 ORL UVA, U-937, and MDA-MB-231 were analyzed using an unpaired two-tailed *t*-test. For cell differentiation analysis, both cell densities and skewness of densities were compared with an unpaired *t*-test. The lowest 5th percentile of densities of differentiated and undifferentiated cells was also compared with a two-tailed *t*-test. *, **, ***, and **** represent $p < 0.05$, $p < 0.01$, $p < 0.001$, and $p < 0.0001$, respectively. Kruskal Wallis and Dunn's tests were performed for the 2D drug test. Viability of cells in 3D drug experiments was analyzed using an unpaired *t*-test with Welch's correction.

RESULTS AND DISCUSSION

Experimental Setup. In this work, the use of a miniaturized lensless microscopy-integrated magnetic levitation platform, HologLev, to monitor and analyze different cell lines was demonstrated by combining two separate technologies to provide low-cost, easy-to-use, and portable cell separation analysis (Figure 1a and Figure S1). The hybrid platform was enclosed in a 3D printed framework that was mainly composed of illumination and acquisition schemes as a slidable one piece and a magnetic levitation section that involves two opposing magnets and a microcapillary channel in between (Figure 1a). Once the sample was placed in the microcapillary between magnets in the platform, heterogeneous cell solution was levitated, and cells reached their equilibrium position when magnetic and buoyancy forces acting on each cell were in equilibrium (Figure 1b). The full field of view (FOV) acquired from the proposed platform serves a far more wider sampling area than that of fluorescence image captured with a 10× microscope objective on an inverted fluorescence microscope for the viability assay using Calcein AM and propidium iodide on MDA-MB-231 cells (Figure 1c). This also illustrated the compatibility of our platform to simply be integrated to a fluorescence microscope by placing a mirror in front of the LED/pinhole scheme for fluorescence acquisition of the same portion of the microcapillary followed by hologram acquisition (Figure S2).

The microspheres and cells residing in the microcapillary channel were analyzed in terms of their levitation heights (i.e., their distance from the top surface of the bottom magnet) under the external magnetic field. After diffraction of the light from the microspheres/cells within the microcapillary channel, the interference pattern composed of the undistorted reference wave and the diffracted object wave was recorded by a CMOS imaging sensor at a distance less than a millimeter. Since there were no optics used between the sample and the imaging sensor, the sample was placed as close as possible to the imaging sensor

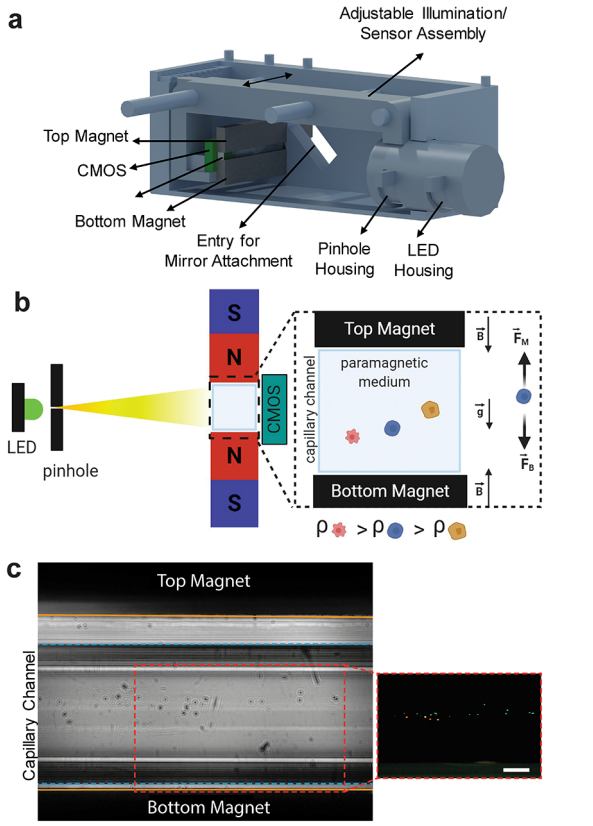

Figure 1. Principles of HologLev. (a) Illustration of the cross-sectional view revealing the interior components. (b) Illustration of the magnetic levitation principle. Particles (or cells) dissolved in a paramagnetic liquid inside the platform come to a unique equilibrium point and levitate under the balance of magnetic force ($\vec{F}_M$) and buoyancy force ($\vec{F}_B$). $\vec{B}$, $\vec{g}$, and ρ represent magnetic induction, gravity, and density, respectively. (c) Comparison of the fields of view between the holographic microscope and fluorescence microscope images of live (green) and dead (red) MDA-MB-231 cells using the mirror attachment in the platform showing magnets (orange lines) and microcapillary channel (blue dashed lines). Scale bar: 200 μm.

to acquire the hologram without the loss of image quality. The spatial resolution was also limited with the pixel size of the imaging sensor (i.e., 1.12 μm). We measured the spatial resolution of our system by imaging a standard optical resolution chart USAF 1951 (Figure S3). Our hybrid platform was capable of resolving features that match with group: 8, element: 1 of USAF 1951 corresponding to 1.95 μm, which was adequate for imaging of mammalian cells whose diameters are greater than the resolved feature size. Thus, quantitative assessment of spatial resolution indicates that the platform not only can have a portable and low-cost design but is also capable of delivering high-resolution images that can compete with high-cost and bulky benchtop microscopes for a wide range of applications from cell imaging to point-of-care-testing. By calibrating using the USAF 1951 resolution chart, the scale on the captured images was set as 0.48 μm/pixel.

Once cells became levitated in the platform, the hologram of the sample was acquired (Figure 2a). The hologram was reconstructed by the Angular Spectrum Method and auto-focusing algorithm (Figure 2b, Video S1). Afterward, the reconstructed image was enhanced digitally and rotated for aligning the bottom magnet horizontally (Figure 2c). After successfully completing these steps, vertical distances (blue line)

https://doi.org/10.1021/acssensors.0c02587
ACS Sens. 2021, 6, 2191−2201

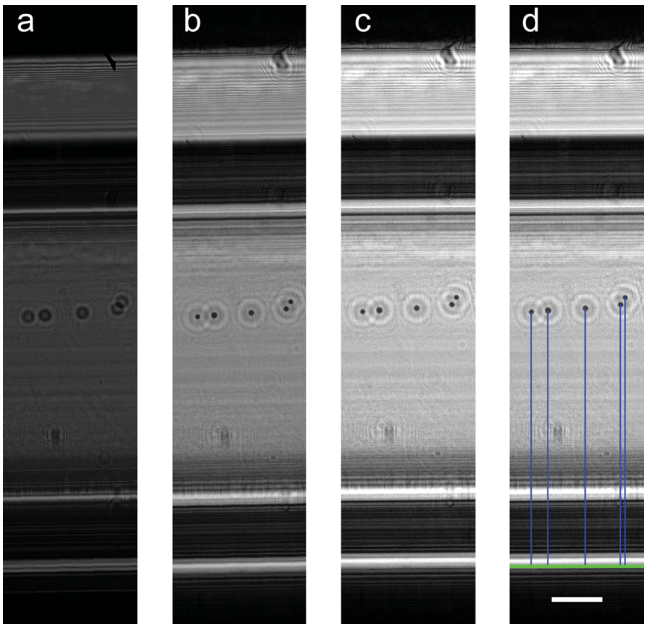

Figure 2. Illustrations of digital image processing steps through determination of relative levitation heights of MDA-MB-231 cells spiked with 100 mM Gd^{3+}. (a) Recorded cell hologram, (b) back-propagated amplitude image, (c) enhancement and rotating of the reconstructed image, and (d) detected cells regarding their relative levitation heights (blue lines) with respect to the bottom magnet (green line). Scale bar: 200 μm.

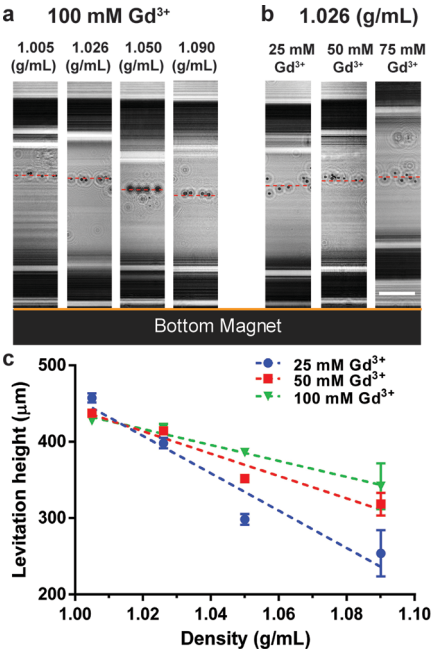

Figure 3. Calibration of HologLev using density-standard microspheres at 1.005, 1.026, 1.05, and 1.09 g/mL densities. (a) Reconstructed images of standard density microspheres at 100 mM Gd^{3+} concentrations. (b) Reconstructed images of 1.026 g/mL microspheres at 25, 50, and 75 mM Gd^{+3} concentrations. Scale bar: 200 μm. (c) Levitation height analyses of different density microspheres under tested Gd^{3+} concentrations (i.e., 25, 50, and 100 mM). Dashed lines represent linear fitting of density versus levitation height data. R^2 values for 25, 50, and 100 mM Gd^{3+} experiments are 0.93, 0.95, and 0.99, respectively. The data are presented as mean ± standard deviation of three different experiments.

of each cell to the bottom magnet (green line) were calculated for determining relative levitation heights of cells that were then converted into density using the calibration curve (Figure 2d). The image processing steps are also shown in Figure S4, and these steps took 2.88 ± 0.37 s processing time from acquiring hologram images to density measurements. In a single hologram image, ~250 cells in average can be analyzed for a concentration of 10^5 cells/mL in a 50 μL capillary tube. Since the image processing steps are rapid, the main part affecting the throughput is the levitation time of 10 min. Because of that, HologLev could reach an analysis throughput of ~5000 cells in ~10 min in a whole capillary. Increasing the cell concentration (i.e., up to 10^6 cells /mL) could decrease the possibility of creating efficient binary masks of cells due to the twin image problem and poor thresholding performance of the image processing algorithm (Figure S5), which can be further improved using an adaptive scheme in future studies. Since the proposed system has low-cost, ease-of-use (automation of the process, preferably no human intervention), and portability features, several platforms could be used in parallel for high-throughput analysis also.

Calibration of the Platform. For cell experiments in HologLev, calibration of the platform was done using polyethylene standard density microspheres (i.e., 1.005, 1.026, 1.050, and 1.090 g/mL). Due to their diamagnetic properties, they migrate from the denser magnetic field regions (i.e., from top and bottom magnets) and levitate at unique heights depending on their density under the balance of magnetic and buoyancy forces. The levitation heights of microspheres were determined automatically from the reconstructed images. Calibration curves obtained with the microspheres' images under different Gd^{3+} concentrations are presented in Figure 3. Almost all microspheres with different densities and Gd^{3+} concentrations showed statistically different levitation heights (Table S1). Density versus levitation height was determined using the standard equations created by fitting the experimental levitation data into linear curves. According to the results, increased Gd^{3+} concentrations caused microspheres to levitate at higher heights and the slope of calibration curves was decreased and so the sensitivity of density analysis. The results were also analyzed by manual counting using a Cell Counter Plugin in ImageJ (Fiji). According to the results, the calibration curve obtained by manual analysis is in good agreement with the calibration curve obtained using automated digital image analysis (Figure S6).

Magnetic Levitation of D1 ORL UVA, U-937, and MDA-MB-231 Cells. Live and dead cells of three different cell lineages (D1 ORL UVA, U-937, and MDA-MB-231) were analyzed within the microcapillary using the magnetic levitation principle. Dead cells of those cell lines were located at the bottom of the capillary channel when a 25 mM Gd^{3+} was used in the levitation medium. To be able to levitate dead cells at higher heights, 100 mM Gd^{3+} was tested (Figure 4a). This Gd^{3+} concentration did not affect cell viability also (Figure S7). We measured the densities of D1 ORL UVA, U937, and MDA-MB-231 cells at 100 mM Gd^{3+} for live to be 1.0721 ± 0.0065, 1.0680 ± 0.0064, and 1.0660 ± 0.0110 g/mL, and for dead to be 1.1653 ± 0.0087, 1.1723 ± 0.0054, and 1.1681 ± 0.0076 g/mL, respectively. At 100 mM Gd^{3+}, the densities of live and dead cells of the same cell line were statistically different when a *t*-test was applied for each of the three cell lines (Figure 4b). In this section, cell death was provided with the introduction of an amphipathic solvent,

https://doi.org/10.1021/acssensors.0c02587
ACS Sens. 2021, 6, 2191−2201

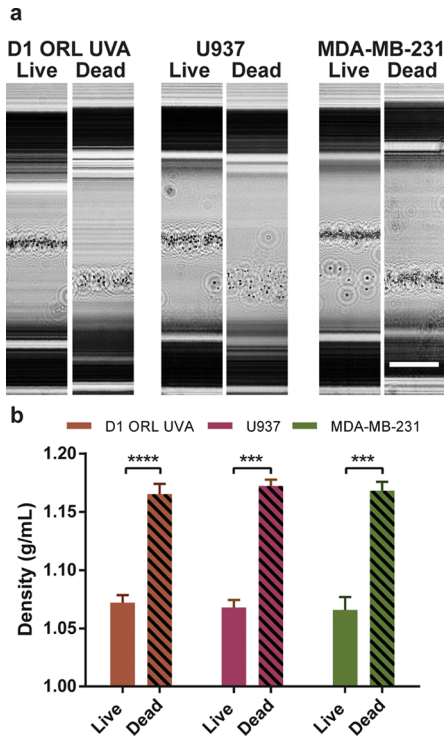

Figure 4. Density analysis of live and dead cells. (a) Reconstructed images and (b) calculated average densities of live and dead D1 ORL UVA, U-937, and MDA-MB-231 cells spiked with 100 mM Gd^{3+}. The data are presented as mean ± standard deviation of three different experiments. The data are compared using an unpaired *t*-test. *** and **** indicate $p < 0.001$ and $p < 0.0001$, respectively. Scale bar: 200 μm.

DMSO, which has cytotoxic effects on cells.[30] DMSO increases cell permeability by interacting with the cells' plasma membrane.[31] Treated and nontreated cells with DMSO for 1 h were also stained with Calcein AM/PI following the manufacturer's instructions to validate the cytotoxic effect on cells (Figure S8). As cell death occurred due to DMSO, disintegration of the cellular structure probably caused accumulation of the Gd-based medium inside the cell. Hence, the effect of the cytoplasm on cell density was eliminated, and the remaining cell debris had a higher density than the intact cell. In our platform, dead cells show high density profiles (1.15 g/mL) than the live cells. The increase in the density profile of dead cells was used for live/dead separation using density gradient centrifugation.[32] We used density gradient centrifugation to separate high-density dead cells (>1.15 g/mL). These cells show a similar levitation profile with the whole dead cell population (Figure S9). Hence, the density changes in dead cell population due to the loss of cell osmolarity can be the main cause of levitation profile change in dead cells. To this end, dead cells were collected at lower heights than the live ones, and thus, the mixture of dead cells and live cells shows clear separation in the levitation platform (Figure S10). These results showed that the change in cell density due to the loss of viability can be effectively identified using HologLev, based on monitoring densities of cells in the channel. Separation of dead cells from the live ones is important in cell-based toxicity assays of pharmaceuticals, environmental contaminants, and other chemicals.[33] In this regard, monitoring dead cells using HologLev would be beneficial to perform portable, real-time, and label-free cell survival analysis with quantitative read-outs for different biomedical applications.

Monitoring Adipogenic Cell Differentiation. Assessment of stem cell differentiation is of great interest in the field of regenerative medicine due to therapeutic potential of stem cells for a variety of diseases ranging from spinal cord injuries to cancer.[34] Thus, it could provide significant advantages to deliver a rapid, low-cost, and portable platform to evaluate differentiated cells from the rest of the population with a minimal need for sample processing and expertise. In a previous study, adipogenic differentiation of bone marrow origin has been reported using a microscope-based magnetic levitation system.[14] To demonstrate our platform's capability to distinguish cell differentiation, similarly, we used 7F2 cells that were treated to adipogenic differentiation using an adipogenic induction medium whereas undifferentiated 7F2 cells were maintained in growth media as control. 7F2 cells were allowed to differentiate by accumulating lipid content within their cytoplasm, which essentially affects the change in density between undifferentiated and differentiated cell populations subject to treatment. Furthermore, adipogenic differentiation of cells exhibits distinct morphological tracks accompanying density change. After the 15th day of cell growth in the culture media for differentiation of 7F2 cells, differentiated and undifferentiated (control) cell solutions were prepared and Gd^{3+} solution corresponding to 25 mM was added to both cell solutions prior to detection of differentiation with our platform. Within 10 min after loading cell solutions to the microcapillary channels, cells reached equilibrium positions and holographic

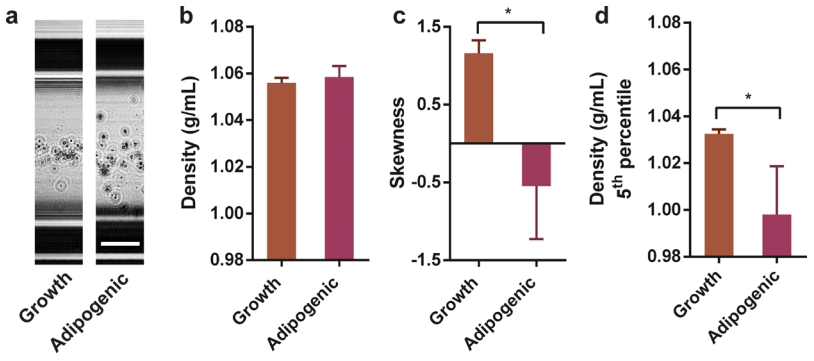

Figure 5. Determination of adipogenic cell differentiation. (a) Reconstructed images of 7F2 (mouse osteoblasts) that were cultured in the growth (7F2G) and adipogenic (7F2A) induction media levitated in 25 mM Gd^{3+} solution. Comparison of (b) average densities, (c) skewness of density for distribution analysis, and (d) the lowest 5th percentile of densities. The data are presented as mean ± standard deviation of three different experiments. The data are compared using an unpaired *t*-test. * indicates $p < 0.05$. Scale bar: 200 μm.

https://doi.org/10.1021/acssensors.0c02587
ACS Sens. 2021, 6, 2191−2201

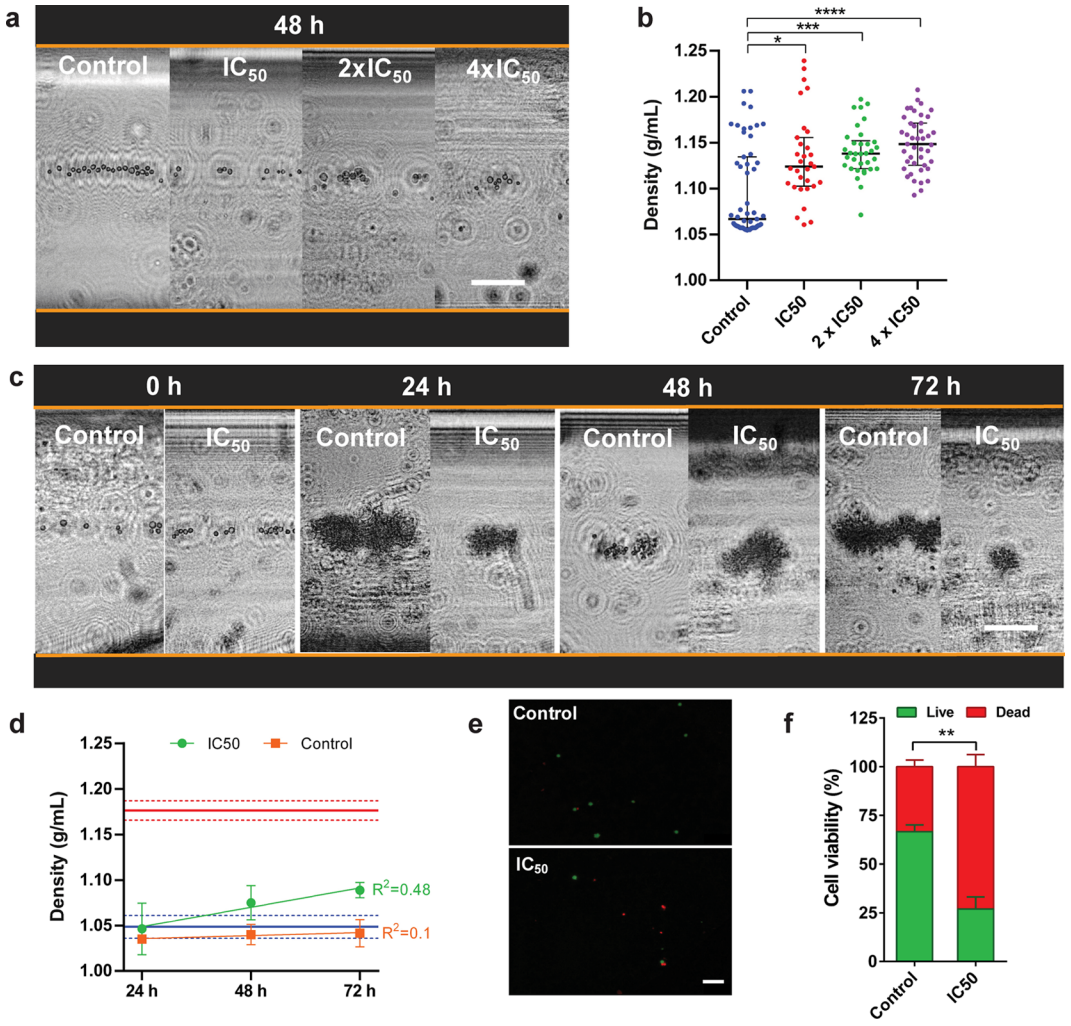

Figure 6. Drug response of levitated MDA-MB-231 cells in 100 mM Gd^{3+} treated with Docetaxel in 2D and 3D incubation environments. (a) Reconstructed holographic images of the levitated cells that were incubated in different drug concentrations ($1 \times IC_{50}$, $2 \times IC_{50}$, $4 \times IC_{50}$) within well-plates for 48 h and (b) the highest 10th percentile of cell densities among these cells. (c) Reconstructed holographic images of the levitated cells that were incubated with and without a drug additive environment in magnetic levitation for 72 h. Scale bar: 200 μm. (d) The measured cell densities for different drug exposure times in the magnetic levitation platform. Blue and red solid lines show the mean cell densities at the beginning of drug exposure (0 h) and the density of cells treated with DMSO for 24 h in the magnetic levitation platform, respectively. Dashed lines correspond to standard deviations of these densities. Linear fits to the data with the coefficient of determination (R^2) are shown as solid green and orange lines. The control group (i.e., without drug) does not show significant correlation. (e) Fluorescence micrographs and (f) the viability analysis of dispersed cells that were levitated for 72 h with and without drug conditions shown in panel (c). *, **, ***, and **** indicate $p < 0.05$, $p < 0.01$, $p < 0.001$, and $p < 0.0001$, respectively. Scale bar: 100 μm.

images of each cell group were acquired. The positions of cells in the microcapillary channel revealed that the average densities of differentiated and undifferentiated (control) cells were similar (Figure 5a,b). However, it seems like differentiated cells occupy a far broad range of levitation heights indicating a more distributed density value (Figure 5c). When undifferentiated and differentiated cells with the lowest density profiles (5th percentile) were compared, undifferentiated cells were shown higher density profiles than the differentiated ones (Figure 5d). Thus, it can be deduced that differentiation induces a decrease in density, and this change dictates the cell to shift toward higher levitation heights. The Red oil O staining results also validated that cells, which were induced with an adipogenic induction agent for 10 days, differentiated into adipocytes (Figure S11). In conclusion, we demonstrated that cell differentiation can be successfully detected with a simple, low-cost, and portable setup with only acquisition and analysis of holographic images that does not require any trained personnel or sophisticated and expensive/time-consuming fluorescence labeling protocols.

Monitoring of 2D and 3D Drug Responses of Cancer Cells. Measuring the drug response is one of the most important and widely studied fields mainly for drug delivery and cancer treatment. So, an effective drug is expected to show an appropriate host response without any adverse side-effects while delivering active molecules to the target biological system. However, it is challenging to measure these effects *in vivo*, and thus, a variety of cell assays are used to assess drug effects on cells by measuring viability, toxicity, etc. Hence, these assays should be deployed with ease and low cost. To provide our systems with capability for drug response monitoring, we conducted experiments with MDA-MB-231 breast cancer cells treated with a common chemotherapy drug, Docetaxel. We progressively tested and compared the effect of the drug in 2D and 3D incubation environments. The dose response curve of Docetaxel

https://doi.org/10.1021/acssensors.0c02587
ACS Sens. 2021, 6, 2191−2201

was studied, and the IC_{50} dose was found to be 63 nM (Figure S12). Afterward, we tested three different drug concentrations (i.e., 63 nM (IC_{50}), 126 nM ($2 \times IC_{50}$), 252 nM ($4 \times IC_{50}$)) on cells grown on well-plates. After 48 h of exposure, cells were collected and analyzed in HologLev (Figure 6a). Even though no significant change was observed in the average cell density in different doses compared to control (Figure S13), the ratios of cells with higher than the average density were increased with drug treatment. When the highest 10th percentile of cell density was selected and compared with control, drug tests showed a significantly increased cell density profile (Figure 6b).

Afterward, we tested the effect of the drug in 72 h cell culture in the magnetic levitation platform forming 3D clusters.[18] In this 3D incubation environment, the pH value of the medium was 8 and remained stable during drug exposure. The IC_{50} dose of Docetaxel was used in these experiments. In the beginning of the experiments (0 h), cells were well-separated and can be distinguishable at the single cell level from acquired holographic images (Figure 6c). Although cells became aggregated in time, they remained levitated in the capillary. We observed that 72 h of drug treatment altered the levitation heights and so the density profile of the cells compared to the control group (Figure 6d). The applied dose evidently adversely affected the viability and boosted the average density of the cells with the drug exposure time. After 72 h of incubation, MDA-MB-231 cells exhibited 1.042 ± 0.015 and 1.089 ± 0.008 g/mL for control and IC_{50} dose, respectively (Figure 6d). Compared to long-term DMSO-treated cells (24 h) (Figure S14), whose densities were measured to be 1.176 ± 0.011 g/mL (red line in Figure 6d), drug-treated cells showed lower density values. On the other hand, compared to the baseline (blue line in Figure 6d) level, drug applied cells showed a gradual, exposure-time dependent increase ($R^2 = 0.48$) in cell densities. Based on cluster composition (live/dead cells), the cluster may locate itself in the direction of the dominant cell group density. In contrast to 2D cytotoxicity assays, our HologLev system facilitated a more physiologically relevant 3D exposure environment.[35] At 72 h, we dispersed all clusters and conducted Calcein AM/PI staining to show that dead cell composition corroborated with the levitation height, where the drug-treated group showed a significantly higher dead cell ratio than the control group (Figure 6e,f). We additionally tested any significant variation of growth medium during 24 h of experiment to manipulate the change in levitation heights of treated cells that may misguide the effect of the drug treatment. Therefore, we used polymeric microspheres with a known density (i.e., the nominal density of the microsphere that the manufacturer indicated is 1.05 g/mL) and levitated them for 24 h in a cell incubator at 37 °C in which the temperature was set the same as in the drug treatment experiments (Figure S15). We verified that levitation height of microspheres was constant for 24 h, which implies that the density change of the medium due to heat and humidity in the incubator is negligible. Consequently, our hybrid platform successfully reveals the density changes in drug-treated cancer cells in a cell culture environment to provide a potential benefit for use in crucial clinical applications without any labeling and expertise for testing drug efficacy while delivering fully automated imaging-based solution.

Density-Based Analysis. Density can be considered as an important physical biomarker to differentiate different cell populations.[6,7] Moreover, the change in the cells' mass to volume ratio may reflect certain cellular processes like cell death,[36] cell differentiation,[37] and the state of disease.[38] In this work, we tested our novel platform for density-based label-free magnetic levitation applications that aims to monitor cells at the single-cell level. Unlike other common single cell analysis methods (i.e., flow cytometry) that require time-consuming and costly labeling protocols of the target cells with additional molecules such as fluorescent antibodies[39] or quantum dots,[40] our platform utilized only the intrinsic label-free biophysical properties of cells. One of the workhorse single-cell sorting techniques, so-called fluorescent-activated cell sorting (FACS) offers tremendous sensitivity for most of the cells with a high throughput (>10,000 cells/s) and provides multiple parameter analysis.[41] Yet, FACS has bottlenecks related to instrumentation costs and the amount of materials used per analysis.[42] Moreover, cell labeling using fluorophore-conjugated antibodies may cause loss of cell viability.[43] On the contrary, magnetic levitation-based tests in HologLev enable cell assays to be done in a portable, low-cost, label-free, and automated manner without affecting the cell viability for the Gd^{3+} concentrations used in this work (i.e., 25−100 mM).[18] Reconstructed holographic images heavily suffer from an artifact called the twin image so that the cell concentration should be sufficiently sparse in order to get well-recovered binary masks to calculate the spatial positions of each microparticle. Since the recent automation framework is sensitive while determining the magnet and capillary positions to exclude irrelevant particles followed by computations of levitation heights, future studies will focus on developing an adaptive and modified thresholding algorithm for holographic imaging that is independent from localized noise around microparticles. Traditional magnetic levitation-based cellular analysis platforms require external imaging equipment (e.g., benchtop microscopes), which not only limits the platform's capability of testing in clinical and home use but also dramatically increases the overall cost of the tests. Thus, we present, for the first time, a standalone magnetic levitation platform with built-in imaging modality that provides high-resolution images (<2 μm) without the need for peripheral optics, auxiliary hardware, and manual optical focusing.[22] Compared to other magnetic levitation-based cell and microparticle-dependent applications with portable imaging modalities,[12,13,22] our design, which combines levitation and holographic imaging, offers high-resolution (i.e., down to 1.95 μm) cell images together with autonomous image processing and cell analysis. The entire platform can be built for less than $100 by using widely accessible and consumable components and can be assembled easily by personnel with intermediate experience in electronics and optics (Table S2). According to the compact design of the device, which is 40 mm × 100 mm × 25 mm, a 3D-printed housing made of polylactic acid (PLA) costs only ~$2. The most expensive components of the platform are the imaging sensor and the microcomputer used for image acquisition, which can be replaced by more compact and low-cost solutions in the oncoming studies.

The importance of fluorescence imaging in point-of-care applications was demonstrated with a portable magnetic levitation device that works in dark field, bright field, and fluorescence imaging modes.[44] With our hybrid design, we also offer the flexibility between holographic and fluorescence imaging (Figure S2), which could be versatile when further validation is necessary depending on the cell type. Although the platform needs a fluorescence microscope for fluorescence imaging, a fluorescence setup could be integrated further into this system.[44,45] HologLev could also be used together with an embedded microcomputer that makes a fully portable and

https://doi.org/10.1021/acssensors.0c02587
ACS Sens. 2021, 6, 2191−2201

pocket-size analysis device like in self-contained[23,46] and cell-phone attachable[21,47] magnetic levitation devices. Magnetic levitation platforms can be also integrated with fluid pumping mechanisms for high-sample-volume analysis,[48] and needless to say, future studies on HologLev will focus on density analysis in continuous flow streams. However, the sample flow rates should be adjusted to get a stable levitation profile and also to get motion blur-free images concerning supporting FPS of the camera for precise measurements of cell levitation heights. In that case, the image processing scheme needs to be adapted also for real-time measurements, which is not indeed an overwhelming software development process. In addition, our platform can also be used for analysis of polymer microspheres that can be applied for point-of-care biomarker quantification by using antibody decorated microspheres.[16]

CONCLUSIONS

Magnetic levitation based on microscopic examination for determining levitation heights of microparticles or cells depends on bench-top microscopes, which are composed of highly fragile and costly optics along with dependency of trained personnel to operate, which limit their usage. In this work, we demonstrated the possible use and practical advantages of the novel hybrid magnetic levitation based LDIHM platform for a variety of applications in life sciences including cell viability, stem cell differentiation, and drug testing. Our novel hybrid magnetic levitation platform showed that it can deliver high-resolution images with a quantitative and fully automated pipeline. The standalone platform has low fabrication cost that can disseminate usage of magnetic levitation technology in different applications. It provides end-to-end automated image acquisition and processing algorithms, which can be further extended to remote and real-time screening of cells to track cellular movement and morphological changes.

ASSOCIATED CONTENT

Supporting Information

The Supporting Information is available free of charge at https://pubs.acs.org/doi/10.1021/acssensors.0c02587.

Figure S1: Illustration of hybrid platform, Figure S2: Illustration of multimodal imaging capability, Figure S3: Spatial resolution achieved with the platform, Figure S4: Image processing pipeline, Figure S5: Digital image processing at high cell concentration, Figure S6: Comparison of manual and automated levitation analysis, Figure S7: The effect of paramagnetic solution on cell viability, Figure S8: Bright field and fluorescence micrographs of control and DMSO treatments, Figure S9: Analysis of dead cells using density gradient centrifugation, Figure S10: Fluorescence micrograph of dead and live cells, Figure S11: Oil red O staining for validation of adipocyte differentiation, Figure S12: Determination of the IC_{50} dose for Docetaxel, Figure S13: Levitation heights of treated cells with Docetaxel in 2D, Figure S14: Reconstructed hologram of levitated cancer cells incubated with DMSO for 24 h, Figure S15: Levitation height change of microspheres for 24 h, Table S1: Statistical analysis of levitation heights of microspheres, Table S2: The prices of the platform components (PDF)

Video of automated hologram back-propagation and density measurement (AVI)

AUTHOR INFORMATION

Corresponding Author

H. Cumhur Tekin − *Faculty of Engineering, Department of Bioengineering, Izmir Institute of Technology, Izmir 35430, Turkey; METU MEMS Center, Ankara 06520, Turkey;* orcid.org/0000-0002-5758-5439; Email: cumhurtekin@iyte.edu.tr

Authors

Kerem Delikoyun − *Faculty of Engineering, Department of Bioengineering, Izmir Institute of Technology, Izmir 35430, Turkey*

Sena Yaman − *Faculty of Engineering, Department of Bioengineering, Izmir Institute of Technology, Izmir 35430, Turkey*

Esra Yilmaz − *Faculty of Engineering, Department of Bioengineering, Izmir Institute of Technology, Izmir 35430, Turkey*

Oyku Sarigil − *Faculty of Engineering, Department of Bioengineering, Izmir Institute of Technology, Izmir 35430, Turkey*

Muge Anil-Inevi − *Faculty of Engineering, Department of Bioengineering, Izmir Institute of Technology, Izmir 35430, Turkey*

Kubra Telli − *Faculty of Science, Department of Molecular Biology and Genetics, Izmir Institute of Technology, Izmir 35430, Turkey*

Ozden Yalcin-Ozuysal − *Faculty of Science, Department of Molecular Biology and Genetics, Izmir Institute of Technology, Izmir 35430, Turkey*

Engin Ozcivici − *Faculty of Engineering, Department of Bioengineering, Izmir Institute of Technology, Izmir 35430, Turkey*

Complete contact information is available at: https://pubs.acs.org/10.1021/acssensors.0c02587

Author Contributions

[‖]K.D. and S.Y. contributed equally to this work and are listed alphabetically. H.C.T. and E.O. conceived and designed the study. K.D. designed and fabricated the platform and developed the automation framework. K.D., S.Y., E.Y., O.S., and K.T. performed the experiments. S.Y. performed the statistical analysis. M.A.-I., O.S., and K.T. performed cell culture. K.D., S.Y., O.S., O.Y.-O., E.O., and H.C.T. analyzed the data. K.D., S.Y., E.Y., E.O., and H.C.T. wrote the manuscript.

Notes

The authors declare no competing financial interest.

ACKNOWLEDGMENTS

The authors would like to thank The Scientific and Technological Research Council of Turkey (119M052) for funding this work. H.C.T. would like to thank Outstanding Young Scientists Award funding (TUBA GEBIP 2020) from the Turkish Academy of Science. K.D. and O.S. acknowledge the support of Turkish Council of Higher Education for 100/2000 CoHE doctoral scholarship. K.D. is thankful for the helpful discussions with Ersin Cine from the Department of Computer Engineering and Ali Aslan Demir from the Department of Photonics at IZTECH while developing the automation framework. We would like to thank Cemre Oksuz from the Department of Bioengineering at IZTECH for kind help in the

analysis of dead cells using density gradient based separation experiments.

REFERENCES

(1) Nayak, S.; Blumenfeld, N. R.; Laksanasopin, T.; Sia, S. K. Point-of-Care Diagnostics: Recent Developments in a Connected Age. *Anal. Chem.* **2017**, *89*, 102−123.

(2) Miyamoto, D. T.; Sequist, L. V.; Lee, R. J. Circulating tumour cells-monitoring treatment response in prostate cancer. *Nat. rev. Clin. Oncol.* **2014**, *11*, 401−412.

(3) Alvarez-Castelao, B.; Schanzenbächer, C. T.; Langer, J. D.; Schuman, E. M. Cell-type-specific metabolic labeling, detection and identification of nascent proteomes in vivo. *Nat. Protoc.* **2019**, *14*, 556−575.

(4) Hao, S. J.; Wan, Y.; Xia, Y. Q.; Zou, X.; Zheng, S. Y. Size-based separation methods of circulating tumor cells. *Adv. Drug Delivery Rev.* **2018**, *125*, 3−20.

(5) Norouzi, N.; Bhakta, H. C.; Grover, W. H. Sorting cells by their density. *PLoS One* **2017**, *12*, e0180520−e0180520.

(6) Bryan, A. K.; Hecht, V. C.; Shen, W.; Payer, K.; Grover, W. H.; Manalis, S. R. Measuring single cell mass, volume, and density with dual suspended microchannel resonators. *Lab Chip* **2014**, *14*, 569−576.

(7) Grover, W. H.; Bryan, A. K.; Diez-Silva, M.; Suresh, S.; Higgins, J. M.; Manalis, S. R. Measuring single-cell density. *Proc. Natl. Acad. Sci.* **2011**, *108*, 10992−10996.

(8) Durmus, N. G.; Tekin, H. C.; Guven, S.; Sridhar, K.; Arslan Yildiz, A.; Calibasi, G.; Ghiran, I.; Davis, R. W.; Steinmetz, L. M.; Demirci, U. Magnetic levitation of single cells. *Proc. Natl. Acad. Sci.* **2015**, *112*, E3661−E3668.

(9) Fuss, I. J.; Kanof, M. E.; Smith, P. D.; Zola, H. Isolation of whole mononuclear cells from peripheral blood and cord blood. *Curr. Protoc. Immunol.* **2009**, *85*, 7.1.1. *Chapter 7*, Unit7.1

(10) Gascoyne, P. R. C. Dielectrophoretic-field flow fractionation analysis of dielectric, density, and deformability characteristics of cells and particles. *Anal. Chem.* **2009**, *81*, 8878−8885.

(11) Ge, S.; Nemiroski, A.; Mirica, K. A.; Mace, C. R.; Hennek, J. W.; Kumar, A. A.; Whitesides, G. M. Magnetic Levitation in Chemistry, Materials Science, and Biochemistry. *Angew. Chem., Int. Ed.* **2020**, *59*, 17810.

(12) Knowlton, S. M.; Yenilmez, B.; Amin, R.; Tasoglu, S. Magnetic Levitation Coupled with Portable Imaging and Analysis for Disease Diagnostics. *J. Visualized Exp.: JoVE* **2017**, *120*, 55012.

(13) Amin, R.; Knowlton, S.; Dupont, J.; Bergholz, J. S.; Joshi, A.; Hart, A.; Yenilmez, B.; Yu, C. H.; Wentworth, A.; Zhao, J. J.; Tasoglu, S. 3D-printed smartphone-based device for label-free cell separation. *J. 3D Print. Med.* **2017**, *1*, 155−164.

(14) Sarigil, O.; Anil-Inevi, M.; Yilmaz, E.; Mese, G.; Tekin, H. C.; Ozcivici, E. Label-free density-based detection of adipocytes of bone marrow origin using magnetic levitation. *Analyst* **2019**, 2942.

(15) Puluca, N.; Durmus, N. G.; Lee, S.; Belbachir, N.; Galdos, F. X.; Ogut, M. G.; Gupta, R.; Hirano, K. I.; Krane, M.; Lange, R.; Wu, J. C.; Wu, S. M.; Demirci, U. Levitating Cells to Sort the Fit and the Fat. *Advanced biosystems* **2020**, *4*, No. e1900300.

(16) Yaman, S.; Tekin, H. C. Magnetic Susceptibility-Based Protein Detection Using Magnetic Levitation. *Anal. Chem.* **2020**, *92*, 12556.

(17) Subramaniam, A. B.; Gonidec, M.; Shapiro, N. D.; Kresse, K. M.; Whitesides, G. M. Metal-amplified Density Assays, (MADAs), including a Density-Linked Immunosorbent Assay (DeLISA). *Lab Chip* **2015**, *15*, 1009−1022.

(18) Anil-Inevi, M.; Yaman, S.; Yildiz, A. A.; Mese, G.; Yalcin-Ozuysal, O.; Tekin, H. C.; Ozcivici, E. Biofabrication of in situ Self Assembled 3D Cell Cultures in a Weightlessness Environment Generated using Magnetic Levitation. *Sci. Rep.* **2018**, *8*, 7239.

(19) Tocchio, A.; Durmus, N. G.; Sridhar, K.; Mani, V.; Coskun, B.; El Assal, R.; Demirci, U. Magnetically Guided Self-Assembly and Coding of 3D Living Architectures. *Adv. Mater.* **2018**, *30*, 1705034.

(20) Sarigil, O.; Anil-Inevi, M.; Firatligil-Yildirir, B.; Unal, Y. C.; Yalcin-Ozuysal, O.; Mese, G.; Tekin, H. C.; Ozcivici, E. Scaffold-free biofabrication of adipocyte structures with magnetic levitation. *Biotechnol. Bioeng.* **2020**, *118*, 1127.

(21) Knowlton, S.; Yu, C. H.; Jain, N.; Ghiran, I. C.; Tasoglu, S. Smart-Phone Based Magnetic Levitation for Measuring Densities. *PLoS One* **2015**, *10*, e0134400−e0134400.

(22) Ozefe, F.; Arslan Yildiz, A. Smartphone-assisted Hepatitis C detection assay based on magnetic levitation. *Analyst* **2020**, *145*, 5816−5825.

(23) Yenilmez, B.; Knowlton, S.; Tasoglu, S. Self-Contained Handheld Magnetic Platform for Point of Care Cytometry in Biological Samples. *Advanced Materials Technologies* **2016**, *1*, 1600144.

(24) Sobieranski, A. C.; Inci, F.; Tekin, H. C.; Yuksekkaya, M.; Comunello, E.; Cobra, D.; von Wangenheim, A.; Demirci, U. Portable lensless wide-field microscopy imaging platform based on digital inline holography and multi-frame pixel super-resolution. *Light, science & applications* **2015**, *4*, e346−e346.

(25) Kecili, S.; Tekin, H. C. Adhesive bonding strategies to fabricate high-strength and transparent 3D printed microfluidic device. *Biomicrofluidics* **2020**, *14*, No. 024113.

(26) Ozcan, A.; McLeod, E. Lensless Imaging and Sensing. *Annu. Rev. Biomed. Eng.* **2016**, *18*, 77−102.

(27) Pech-Pacheco, J. L.; Cristobal, G.; Chamorro-Martinez, J.; Fernandez-Valdivia, J. Diatom autofocusing in brightfield microscopy: a comparative study. In *Proceedings 15th International Conference on Pattern Recognyition. ICPR-2000*; IEEE: 3−7 Sept. 2000; 2000 pp. 314−317, *3*.

(28) Duda, R. O.; Hart, P. E. Use of the Hough transformation to detect lines and curves in pictures. *Commun. ACM* **1972**, *15*, 11−15.

(29) Illingworth, J.; Kittler, J. A survey of the hough transform. *Computer Vision, Graphics, and Image Processing* **1988**, *44*, 87−116.

(30) de Abreu Costa, L.; Henrique Fernandes Ottoni, M.; Dos Santos, M. G.; Meireles, A. B.; Gomes de Almeida, V.; de Fátima Pereira, W.; Alves de Avelar-Freitas, B.; Eustáquio Alvim Brito-Melo, G. Dimethyl Sulfoxide (DMSO) Decreases Cell Proliferation and TNF-α, IFN-γ, and IL-2 Cytokines Production in Cultures of Peripheral Blood Lymphocytes. *Molecules* **2017**, *22*, 1789.

(31) Notman, R.; Noro, M.; O'Malley, B.; Anwar, J. Molecular Basis for Dimethylsulfoxide (DMSO) Action on Lipid Membranes. *J. Am. Chem. Soc.* **2006**, *128*, 13982−13983.

(32) Kovacovicova, K.; Vinciguerra, M. Isolation of senescent cells by iodixanol (OptiPrep) density gradient-based separation. *Cell Proliferation* **2019**, *52*, No. e12674.

(33) Fritzsche, M.; Mandenius, C.-F. Fluorescent cell-based sensing approaches for toxicity testing. *Anal. Bioanal. Chem.* **2010**, *398*, 181−191.

(34) Han, Y.; Li, X.; Zhang, Y.; Han, Y.; Chang, F.; Ding, J. Mesenchymal Stem Cells for Regenerative Medicine. *Cell* **2019**, *8*, 886.

(35) Eilenberger, C.; Rothbauer, M.; Selinger, F.; Gerhartl, A.; Jordan, C.; Harasek, M.; Schädl, B.; Grillari, J.; Weghuber, J.; Neuhaus, W.; Küpcü, S.; Ertl, P. A Microfluidic Multisize Spheroid Array for Multiparametric Screening of Anticancer Drugs and Blood−Brain Barrier Transport Properties. *Adv. Sci.* **2021**, *n/a*, 2004856.

(36) Martin, S. J.; Bradley, J. G.; Cotter, T. G. HL-60 cells induced to differentiate towards neutrophils subsequently die via apoptosis. *Clin. Exp. Immunol.* **1990**, *79*, 448−453.

(37) Maric, D.; Maric, I.; Barker, J. L. Buoyant density gradient fractionation and flow cytometric analysis of embryonic rat cortical neurons and progenitor cells. *Methods* **1998**, *16*, 247−259.

(38) Mrema, J. E.; Campbell, G. H.; Miranda, R.; Jaramillo, A. L.; Rieckmann, K. H. Concentration and separation of erythrocytes infected with Plasmodium falciparum by gradient centrifugation. *Bull World Health Organ.* **1979**, *57*, 133−138.

(39) Herzenberg, L. A.; Parks, D.; Sahaf, B.; Perez, O.; Roederer, M.; Herzenberg, L. A. The history and future of the fluorescence activated cell sorter and flow cytometry: a view from Stanford. *Clin. Chem.* **2002**, *48*, 1819−1827.

(40) Chattopadhyay, P. K., Chapter 18 - Quantum Dot Technology in Flow Cytometry. In *Methods in Cell Biology*; Darzynkiewicz, Z.; Holden,

https://doi.org/10.1021/acssensors.0c02587
ACS Sens. 2021, 6, 2191−2201

E.; Orfao, A.; Telford, W.; Wlodkowic, D., Eds. Academic Press: 2011; Vol. *102*, pp. 463−477.
(41) Ashcroft, R. G.; Lopez, P. A. Commercial high speed machines open new opportunities in high throughput flow cytometry (HTFC). *J. Immunol. Methods* **2000**, *243*, 13−24.
(42) Hu, P.; Zhang, W.; Xin, H.; Deng, G. Single Cell Isolation and Analysis. *Front. Cell Dev. Biol.* **2016**, *4*, 116.
(43) Kumar, A.; Bhardwaj, A. Methods in cell separation for biomedical application: cryogels as a new tool. *Biomedical materials (Bristol, England)* **2008**, *3*, No. 034008.
(44) Knowlton, S.; Joshi, A.; Syrrist, P.; Coskun, A. F.; Tasoglu, S. 3D-printed smartphone-based point of care tool for fluorescence- and magnetophoresis-based cytometry. *Lab Chip* **2017**, *17*, 2839−2851.
(45) Sencan, I.; Coskun, A. F.; Sikora, U.; Ozcan, A. Spectral Demultiplexing in Holographic and Fluorescent On-chip Microscopy. *Sci. Rep.* **2015**, *4*, 3760.
(46) Yenilmez, B.; Knowlton, S.; Yu, C. H.; Heeney, M. M.; Tasoglu, S. Label-Free Sickle Cell Disease Diagnosis using a Low-Cost, Handheld Platform. *Adv. Mater. Technol.* **2016**, *1*, 1600100.
(47) Knowlton, S. M.; Sencan, I.; Aytar, Y.; Khoory, J.; Heeney, M. M.; Ghiran, I. C.; Tasoglu, S. Sickle cell detection using a smartphone. *Sci. Rep.* **2015**, *5*, 15022−15011.
(48) Amin, R.; Knowlton, S.; Yenilmez, B.; Hart, A.; Joshi, A.; Tasoglu, S. Smart-phone attachable, flow-assisted magnetic focusing device. *RSC Adv.* **2016**, *6*, 93922−93931.

https://doi.org/10.1021/acssensors.0c02587
ACS Sens. 2021, 6, 2191−2201